coatings

MDPI

Article

Hydrogenation Behavior of Cr-Coated Resistance Upset Welds of E110 Zirconium Alloy

Egor Kashkarov *, Kirill Gusev, Viktor Kudiiarov, Nikita Kurdyumov and Dmitrii Sidelev

School of Nuclear Science and Engineering, National Research Tomsk Polytechnic University, 634050 Tomsk, Russia

* Correspondence: egor_kashkarov@mail.ru; Tel.: +7-3822-70-17-77 (ext. 1562)

Abstract: The hydrogenation behavior of Cr-coated resistance upset welds (RUW) of E110 zirconium alloy was investigated at 360, 450 and 900 °C and a hydrogen pressure of 2 bar. The deposition of Cr coating, via magnetron sputtering, can decrease the hydrogen absorption rate of an RUW Zr alloy. The activation energy for the hydrogen absorption of Cr-coated specimens (84 kJ/mol) is higher in comparison with uncoated ones (71 kJ/mol), which indicates the deceleration of the hydriding of welded Zr alloys in the case of Cr coating deposition. A Cr coating can limit the formation of radially oriented hydrides and the hardening of RUW specimens at 360 and 450 °C. No significant difference in the hydrogen absorption rate was found at 900 °C. The application of Cr coating deposition to protect resistance-upset-welded Zr alloys in a hydrogen atmosphere is discussed.

Keywords: resistance upset welding; hydrogenation; zirconium alloys; chromium; coating; accident tolerant fuel

Citation: Kashkarov, E.; Gusev, K.; Kudiiarov, V.; Kurdyumov, N.; Sidelev, D. Hydrogenation Behavior of Cr-Coated Resistance Upset Welds of E110 Zirconium Alloy. *Coatings* **2023**, *13*, 339. https://doi.org/10.3390/coatings13020339

Academic Editor: Jinyang Xu

Received: 29 December 2022
Revised: 24 January 2023
Accepted: 31 January 2023
Published: 2 February 2023

1. Introduction

Fuel claddings are the first physical barrier to exclude an output of uranium fuel in an active zone of light-water nuclear reactors. Zirconium alloys are base materials for nuclear fuel claddings due to their relevant functional properties such as a low thermal neutron capture cross-section (0.02 b), high corrosion and radiation resistance, and acceptable mechanical properties [1,2]. However, the last nuclear accident that occurred in 2011 at the Fukushima Daiichi nuclear power plant pointed out the critical weakness of Zr alloys in water steam under high temperatures [3,4]. The interaction of zirconium alloys with water steam can result in its rapid oxidation, the generation of gaseous hydrogen, and the hydrogenation of zirconium alloys. It is more important that the reaction of Zr alloy claddings with water steam has exothermic behavior which leads to the overheating of the cladding [5]. Thereby, Zr alloy claddings can be strongly oxidized and hydrogenated under high temperatures in the case of a loss of coolant accident (LOCA) with a resultant decrease in its plasticity and embrittlement with future swelling and bursting.

The deposition of a protective coating on the outer surface of Zr fuel claddings is suggested as a possible way to increase the "coping time" before the embrittlement and failure of fuel claddings. To date, metals (Cr) [6] and compound (TiN, CrN, SiC, CrC) [7,8], multicomponent (FeCrAl, AlCrY, (AlTiCrNiTa)N, CrAl) [9–11], and multilayer (Cr/CrN, Cr/ZrO_2) [12–14] coatings have been studied as candidate materials to improve the oxidation resistance of Zr alloys. Among many coating materials, chromium can be selected as more relevant due to its acceptable thermal neutron cross-section, relevant mechanical properties, and the formation of dense and stable oxide scales in supercritical water and under LOCA conditions. The deposition of Cr coatings on the outer surface of Zr alloy claddings also results in increasing corrosion properties under normal operation conditions (~360 °C, 18.6 MPa) [15]. Many laboratory tests and full-scale experiments demonstrated enhanced oxidation resistance of Cr-coated Zr alloys in water steam in comparison with

uncoated ones. The crucial problem of Cr-coated Zr alloys consists of the growth of a eutectic Cr-Zr layer (with a melting point of 1332 °C [14]) under high-temperature oxidation, leading to the fast failure of coated Zr alloy claddings. Despite this, some experiments have aimed to evaluate the adhesion and cracking resistance of Cr coatings onto Zr alloys [16] to determine their service properties.

It is no less important to define the hydrogenation behavior of coated Zr alloys under normal operation and LOCA conditions. The formation of hydrides in Zr alloy claddings can cause a significant change in mechanical properties due to its orientations in circumferential and/or plane directions or even in the case of homogeneous distribution [17]. The concentration of absorbed hydrogen in Zr alloys can depend on their microstructure and the mechanical properties of the prior β-Zr phase that can be formed during the cooling stage from high temperatures [18–20]. Taking into account the fact that Zr alloy fuel rods are produced by welding end plugs to a cladding tube at both sides, the effect of welding and next coating deposition on the hydrogenation behavior of Zr alloys should be also considered. Several studies have already shown the decrease in the hydrogen pick up of coated Zr alloys under normal operation temperatures [21–24]. However, different types of welding are used in the nuclear industry for the treatment of Zr alloy claddings. Laser beam welding (LBW) can be applied to join spacer grids, while resistance upset welding (RUW) is commonly used to weld ends and fuel tubes to produce Zr fuel claddings. The authors previously investigated the hydrogenation behavior of Cr-coated laser beam welds made from an E110 zirconium alloy under normal operation and at an elevated temperature in hydrogen atmosphere [25]. The influence of other types of Zr alloy welding and next coating deposition should be analyzed to determine the need to apply a Cr coating to protect the ends and welds of nuclear fuel rods. The aim of this paper is to determine the role of Cr coating on the hydrogenation behavior of RUW Zr alloy specimens at normal operation and LOCA temperatures.

2. Materials and Methods

2.1. Specimen Preparation

Specimens (Figure 1) were produced using the standard technology of resistance upset welding of a Zr alloy cladding tube with an end plug in the public joint-stock company "Novosibirsk Chemical Concentrates Plant" (NCCP, Rosatom, Novosibirsk, Russia). The cladding tube (diameter of Ø9.1 mm, wall thickness of 0.55 mm) and end plug made from an E110 (0.9–1.1 wt% Nb, 0.06–0.1 wt% O and Zr balance) zirconium alloy were used as original materials to produce specimens. The first series of specimens was as-received (uncoated), which did not undergo any post-treatment operations after welding. The second series of specimens were coated by chromium using multi-cathode magnetron sputtering. Special substrate holders were used to fix specimens from one edge for coating deposition. Due to this, the outer surface of the specimens was fully coated, while an inner area of the tubes remained uncoated. Prior to the coating process, specimens of the second series were etched by Ar^+ ions for 20 min to delete surface contaminations. The following parameters of ion source were used: accelerated voltage of 2.5 kV, ion current of 40 mA, and Ar pressure of 0.1 Pa. The procedure of Cr coating deposition was the same as it was in previous studies [26,27]. The obtained Cr coating had a dense and columnar microstructure with a uniform thickness of ~9.8 ± 0.4 μm. Other parameters of such a type of Cr coating can be found in ref. [27] (specimen M8.2).

An automated machine Gas Reaction Controller (GRC) was used to perform the gas phase hydrogenation of the specimens at 360, 450 and 900 °C. The vacuum chamber was evacuated up to a pressure of 10^{-3} Pa and then heated up to the given temperature. The heating rate was equal to 6 °C/min. After the heating stage, hydrogen (99.9999%) was injected into the chamber. The hydrogen pressure was maintained as constant (2 bar). The duration of hydrogenation for Cr-coated and uncoated specimens was 240, 35 and 5 min at 360, 450 and 900 °C, respectively. The absorbed hydrogen was recorded during each hydrogenation test. After hydrogenation, the chamber was evacuated, and specimens

cooled down up to room temperature with a rate of ~5–10 °C/min. An analytical balance machine (Sartorius CP124 S with an accuracy of 10^{-4} g) was used to measure the weight gain of specimens before and after the hydrogenation tests.

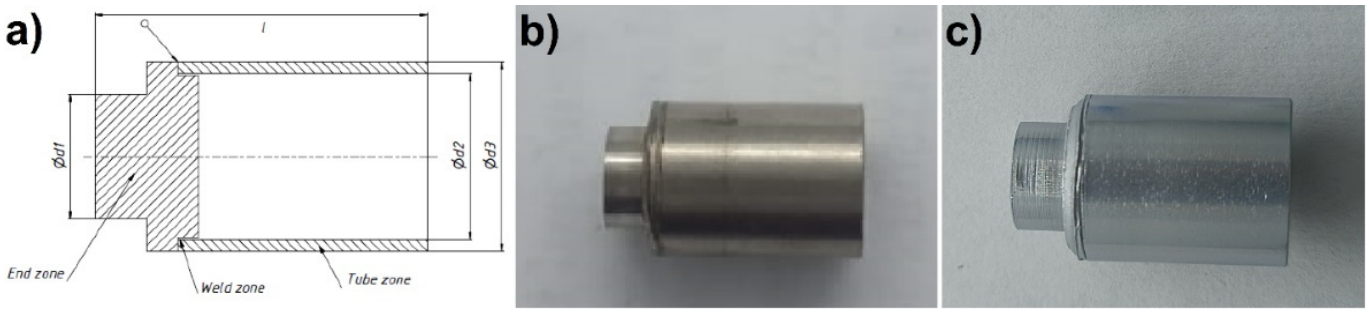

Figure 1. The schematic drawing of an RUW specimen (**a**). Appearance of (**b**) uncoated and (**c**) Cr-coated RUW E110 alloy specimens before hydrogenation tests.

2.2. Hydrogenation Tests

2.3. Specimen Characterization

The cross-section microstructure of RUW E110 alloy specimens after the hydrogenation tests was investigated using an optical microscopy via AXIOVERT-200 MAT (Zeiss, Jena, Germany). The phase composition of specimens was analyzed in their cross-section via X-ray diffraction (XRD) using XRD-7000S (Shimadzu, Kyoto, Japan) with CuK_α radiation (30 kV, 40 mA). The identification and calculation of phase composition by Rietveld refinement were performed using the ICCD-4+ database and the SIeve program. The hardness of specimens was studied in the end plug (EZ), weld (WZ) and tube (TZ) zones. Hardness measurements were performed on cross-sections of specimens using the Nanohardness Tester 2 (CSM, Geneva, Switzerland). The indentation load and distance between indentations were equal to 100 mN and ~100 μm, respectively. Thirty indentations were performed in each zone of all specimens; then, hardness was averaged for each zone.

3. Results

3.1. Hydrogenation Tests

Hydrogen absorption curves for two series of RUW specimens (uncoated and Cr-coated) at different temperatures are shown in Figure 2. For both specimens, hydrogen absorption increased with the temperature of the hydrogenation tests. It was shown that hydrogen absorption is lower in the case of Cr-coated RUW E110 alloy specimens compared to uncoated ones. Hydrogen absorption rates (q) were calculated from a slope of curves (Figure 2) and presented in Table 1.

The deposition of Cr coating on RUW specimens led to a decrease in its hydrogen absorption rate by 7.5 times at 360 °C, 8.5 times at 450 °C, and 3.8 times at 900 °C (Table 1). The hydrogen absorption by the uncoated RUW specimen was characterized by a linear growth of hydrogen concentration up to 0.007 wt.% at 360 °C (until 120 min). Then, the hydrogen absorption of the uncoated specimen accelerated due to a reduction in the surface oxide film by hydrogen (Figure 2a) [28]. When the temperature of the hydrogenation tests was 450 °C, the near-linear growth of hydrogen concentration was observed for both types of specimens during the entire hydrogenation period (Figure 2b). However, the absorbed hydrogen concentration was significantly lower for the Cr-coated RUW E110 alloy. Similar behaviors of the hydrogen absorption kinetics of the uncoated and Cr-coated RUW specimens were observed at 900 °C (Figure 2c), but the Cr-coated RUW specimen had a lower absorption rate. Nevertheless, the hydrogen absorption rate increased significantly at 900 °C, even for the Cr-coated specimen ($9.8 \cdot 10^{-2}$ $cm^3(H_2) \cdot cm^{-2} \cdot s^{-1}$). It can be observed that the absorption curve for the uncoated RUW specimen showed a significant decrease in the hydrogen absorption rate at a hydrogen concentration above 0.8 wt.% (Figure 2c). This indicates the decrease in absorption rate was caused by the formation of δ-zirconium

hydrides, which have a lower hydrogen diffusion rate [25,29,30]. At the same time, the Cr-coated RUW specimen showed a smoother change in the hydrogen absorption rate.

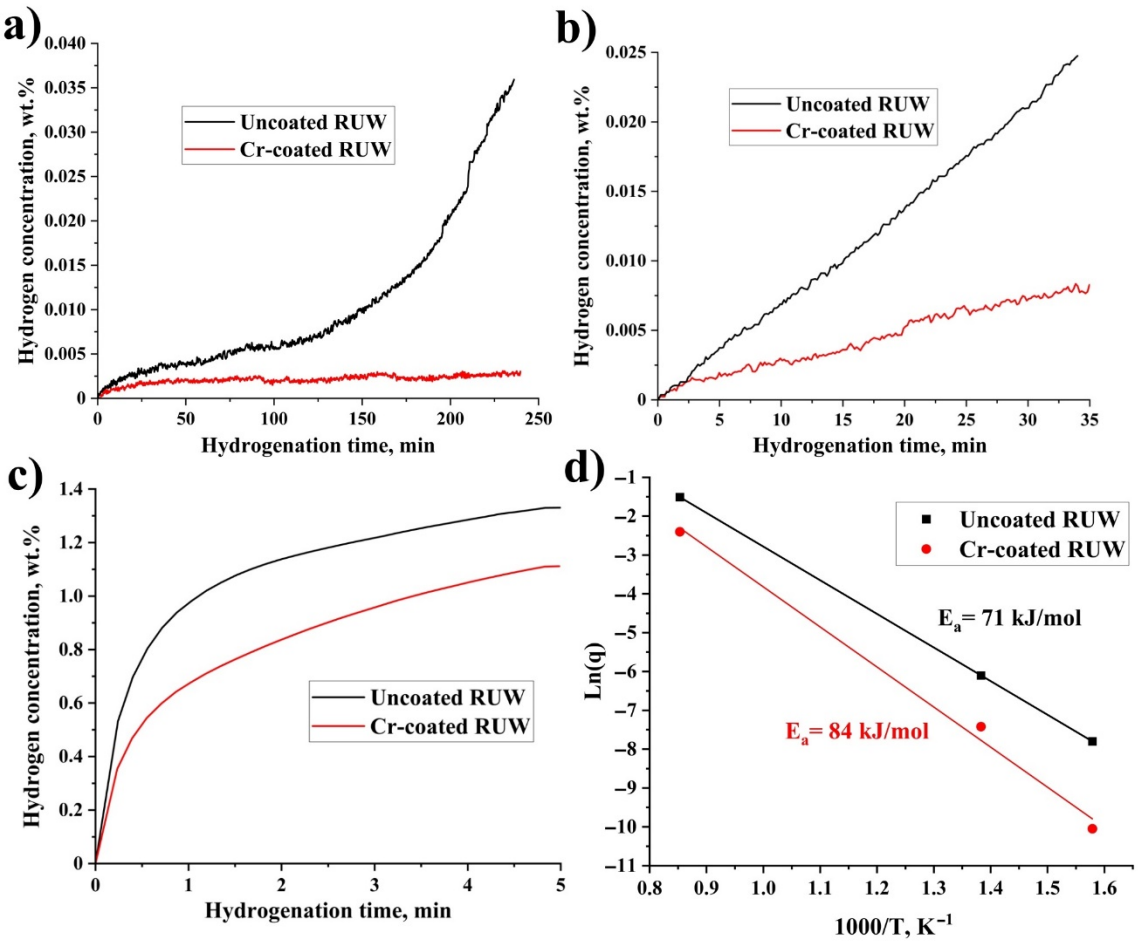

Figure 2. Hydrogen absorption curves for uncoated and Cr-coated RUW E110 alloy specimens at (**a**) 360, (**b**) 450, and (**c**) 900 °C. (**d**) Arrhenius plots for uncoated and Cr-coated RUW specimens.

Table 1. Hydrogen absorption rate for uncoated and Cr-coated RUW E110 alloy specimens.

Time, Min	*T*, °C	Hydrogen Absorption Rate (q), $cm^3(H_2)\cdot cm^{-2}\cdot s^{-1}$		Hydrogen Concentration (C_H), ppm	
		Cr-Coated RUW	Uncoated RUW	Cr-Coated RUW	Uncoated RUW
240	360	$2.8\cdot10^{-5}$	$2.1\cdot10^{-4}$	30	240
35	450	$2.7\cdot10^{-4}$	$2.3\cdot10^{-3}$	64	890
5	900	$9.8\cdot10^{-2}$	$3.7\cdot10^{-1}$	3900	2700

Arrhenius curves were plotted for a comparative analysis of activation energy for the hydrogen absorption of the uncoated and Cr-coated RUW specimens (Figure 2d). The obtained values also confirmed the barrier properties of the Cr coating: the activation energy of hydrogen absorption was higher for Cr-coated specimens (84 kJ/mol) compared to uncoated ones (71 kJ/mol). The activation energy of sorption and desorption was the minimum amount of energy that hydrogen molecules need to receive for their dissociation on the surface of a substance (to overcome the activation barrier) or hydrogen atoms for their recombination into molecules and desorption. The value of activation energy is the minimum amount of energy that needs to be supplied to the system (joule per mole) for a sorption/desorption reaction to occur. Thus, an increase in the value of the activation energy of hydrogen sorption by 18% due to the chromium coating deposition on the welded zirconium alloy indicated an increase in the hydrogen resistance of the alloy due to a decrease in the rate of hydrogenation.

3.2. Phase Composition and Cross-Section Microstructure of RUW Specimens

The phase composition of RUW specimens is presented in Figure 3. The as-received RUW specimen was represented only by an α-Zr phase. The analysis of XRD patterns shows the formation of the δ-$ZrH_{1.66}$ hydride phase in the uncoated RUW specimens hydrogenated at all temperatures. The intensities of the δ phase reflections increased with temperature, which indicated higher content of the hydride phase and correlated with the measured H concentrations in specimens. For Cr-coated specimens, the formation of two types of hydrides (δ-$ZrH_{1.66}$ and γ-ZrH) was observed only after hydrogenation at 900 °C, despite the fact that the hydrides were clearly seen in optical images for the coated specimen hydrogenated at 450 °C (Figure 4). This was due to the low concentration of hydrogen and, therefore, hydrides in the sample, which made it difficult to detect via the XRD technique. It should be noted that the specimens were analyzed on cross-sections, and no reflections from the thin Cr coating were also observed in the XRD patterns of the Cr-coated specimens.

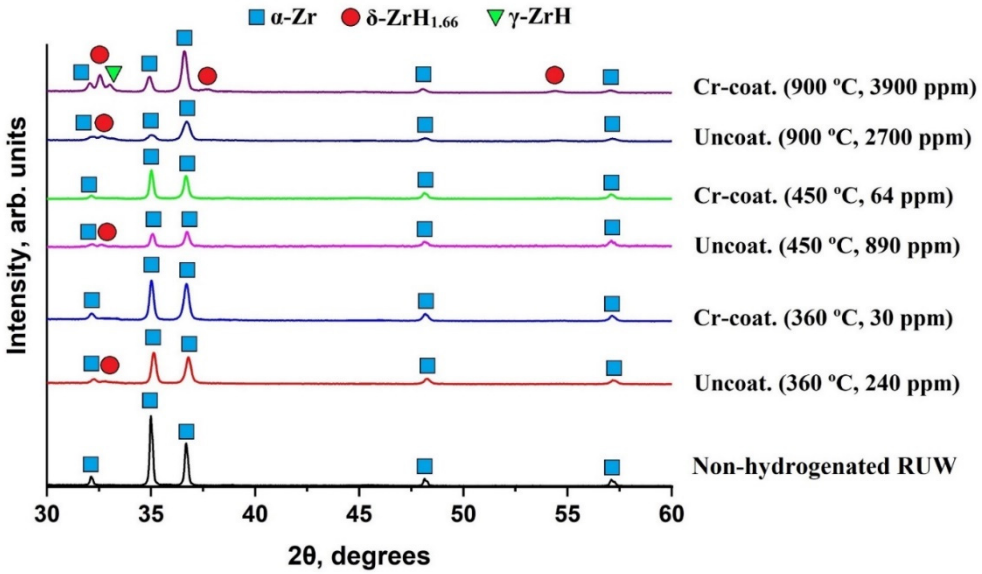

Figure 3. XRD patterns of Cr-coated and uncoated RUW specimens after hydrogenation test.

Figure 4 shows cross-section optical images of specimens after the hydrogenation tests. The microstructural analysis showed that Cr-coated specimens did not have cracks or hydrides in all observed zones at a temperature of 360 °C. No peeling of Cr coatings was found. At the same temperature, the uncoated RUW specimen had cracks formed at the welding burr.

Precipitations of hydrides (dark contrast) were observed inside the Cr-coated specimen at 450 °C. Hydrides have different orientations: they are primarily circumferentially on the outer side of the specimen, while they are radially orientated on the inner side. Radially oriented hydrides can cause an undesirable path of crack propagation, leading to the brittle fracture of the cladding material [31]. Hydrides also precipitate along a weld zone, and here, some reorientation of hydrides in a direction to the outer surface of the weld zone was observed. The same orientations were observed for the uncoated specimen at 360 and 450 °C, which was caused by hydrogen diffusion from the inner uncoated side. Moreover, a hydride rim was also observed inside uncoated specimens on the outer side, also found in [32].

Due to the high diffusion mobility of hydrogen at 900 °C, both uncoated and Cr-coated RUW specimens had relatively uniform distributions and high contents of hydrides inside the volume of the specimens. It was found that the Cr-coated specimen had a higher hydride concentration than the uncoated one.

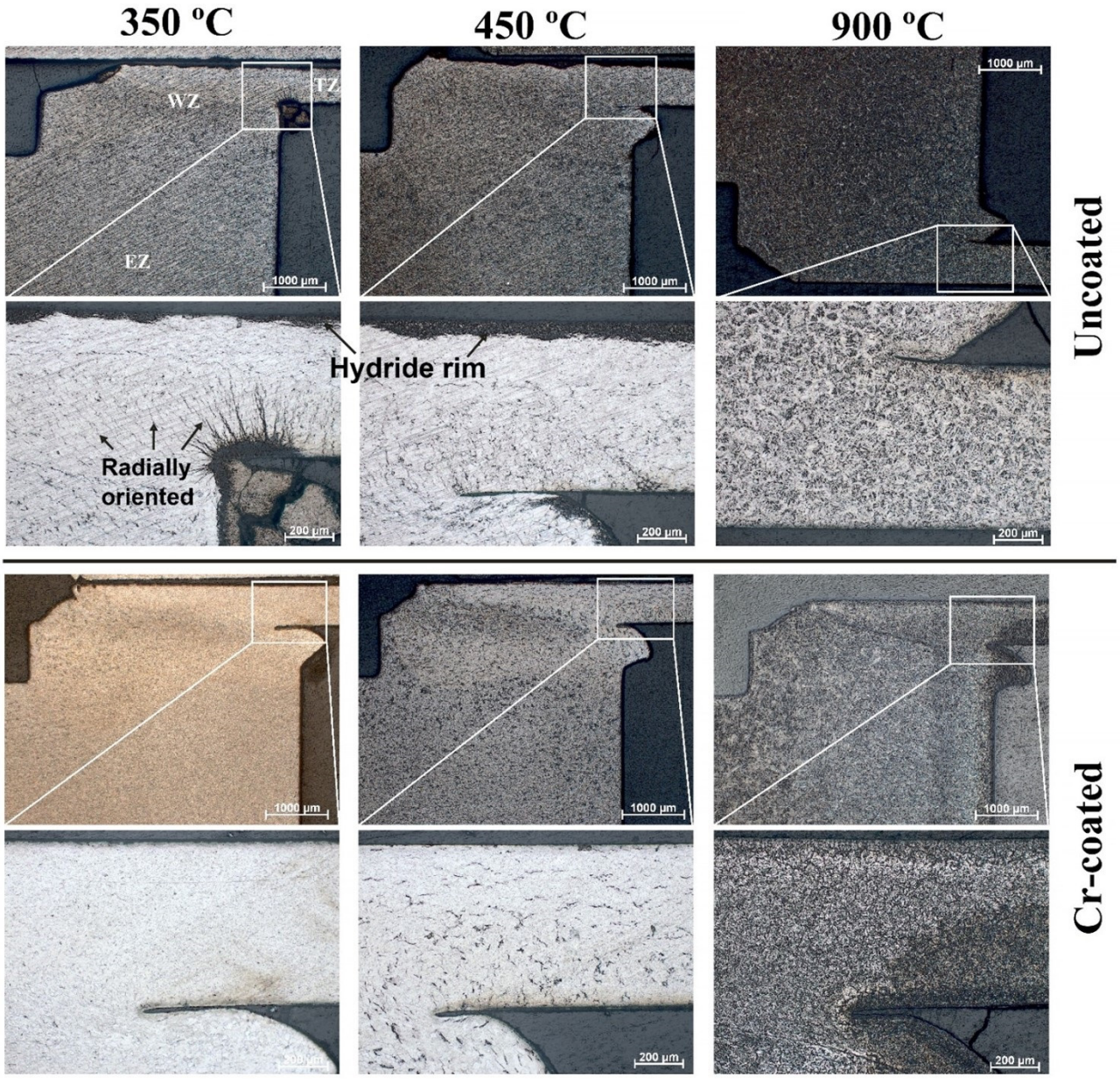

Figure 4. Optical images of cross-section microstructure of Cr-coated and uncoated RUW specimens after hydrogenation tests at 360, 450, and 900 °C.

Figure 5 shows cross-section optical images of specimens in a TZ. It was found that the increase in hydrogenation temperature could lead to a formation of a hydride rim. This was observed for uncoated specimens at 360 and 450 °C, while the hydride rim was not observed for Cr-coated specimens after all the hydrogenation tests. When the hydride rim was formed (at a depth of ~50 µm), hydrogen still penetrated further into the alloy, where hydrides are formed. For both types of specimens at 900 °C, absorption and diffusion rates were high, so hydride formation occurred throughout a volume of specimens.

3.3. Hardness Measurements

The hardness of the uncoated and Cr-coated RUW specimens is shown in Table 2. The hardness of the as-received RUW E110 alloy had a uniform distribution, and the obtained values of hardness were comparable with that of E110 zirconium alloy (~180 HV) [33]. According to Table 2, the magnetron deposition of the Cr coating on the outer surface of the RUW E110 alloy did not affect its hardness using the applied deposition parameters. The

maximal temperature of the RUW alloy during Cr coating deposition (390 °C) was less than the typical annealing temperature of Zr alloy cladding tubes and welds (500–580 °C) [34,35].

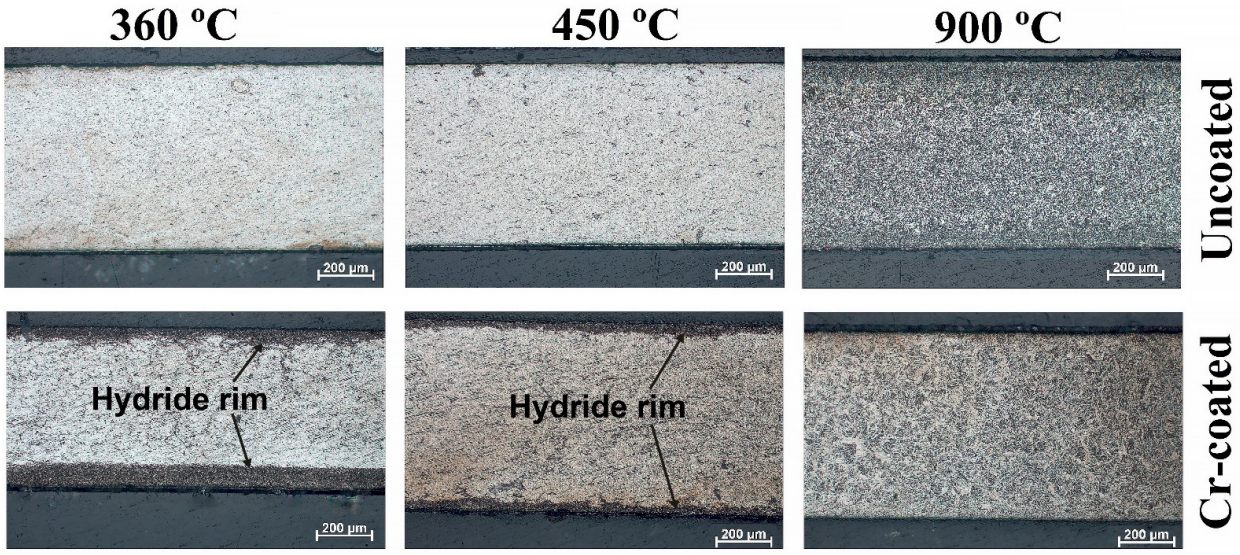

Figure 5. Cross-section optical images of uncoated and Cr-coated RUW E110 alloy specimens in tube zones.

Table 2. Hardness of uncoated and Cr-coated RUW E110 alloy specimens.

Specimen	Time, Min	T, °C	C_H, ppm	Average Hardness, HV		
				EZ	WZ	TZ
As-received Cr-coated	0	0	0	210 ± 17	212 ± 19	191 ± 14
As-received uncoated	0	0	0	208 ± 30	213 ± 10	178 ± 9
Cr-coated	240	360	30	208 ± 30	220 ± 24	207 ± 33
Uncoated	240	360	240	232 ± 37	255 ± 41	273 ± 36
Cr-coated	35	450	64	218 ± 24	212 ± 26	216 ± 19
Uncoated	35	450	890	223 ± 37	229 ± 32	231 ± 50
Cr-coated	5	900	3900	266 ± 27	270 ± 30	260 ± 42
Uncoated	5	900	2700	266 ± 26	255 ± 20	266 ± 32

The hydrogenation of RUW specimens led to the hardening of both types of specimens (Cr-coated and uncoated) due to a formation of the δ-ZrH phase. After the hydrogenation test at 360 °C, the hardness of the uncoated RUW specimen was equal to 255 HV in WZ, while the Cr-coated one had 220 HV in the same zone. The hardness of the uncoated RUW specimen (229 HV) was also higher in WZ at 450 °C compared to that of the Cr-coated RUW (212 HV). The hardness of specimens was the highest (255–270 HV) in all zones after the hydrogenation tests at 900 °C. At the same time, the hardness in WZ became higher for the Cr-coated specimen due to the higher hydrogen concentration compared to the uncoated specimen (3900 and 2700 ppm, respectively).

4. Discussion

The hydrogenation of resistance upset welds (RUW) from E110 zirconium alloy was performed at 360, 450, and 900 °C. It was shown that native surface oxide can limit the penetration of hydrogen to the welded alloy to some extent (Figure 2a). However, when such an oxide layer was reduced, the hydrogen absorption rate rapidly accelerated. At higher temperatures (450 and 900 °C), the hydrogenation absorption rate of the uncoated specimens drastically increased (from $2.1 \cdot 10^{-4}$ to $2.3 \cdot 10^{-3}$ and $3.7 \cdot 10^{-1}$ cm^3 $(H_2) \cdot cm^{-2} \cdot s^{-1}$,

respectively). A hydride rim could be formed in the outer surface of the welded alloy at 360 and 450 °C. The tube zones of uncoated RUW specimens preferred circumferentially oriented hydrides (Figure 5), while hydrides formed in the radial direction in the weld zone of specimens. The phase transformation of α-Zr into δ-$ZrH_{1.66}$ could lead to a volume expansion of about 17.2% [36]. Possible stress concentrations can be easily released in brittle hydride precipitates and at the α/δ phase boundaries [37]. The latter can lead to a negative effect on the mechanical properties of welded specimens [25]. Indeed, the noticeable increase in the hardness of RUW specimens after hydrogenation was determined (Table 2). After hydrogenation at 900 °C, the uncoated RUW specimen had a uniform distribution of hydrides throughout the volume of specimens. As hydrogen solubility and diffusivity can drastically increase in Zr alloys at high temperatures [38], no hydrogen rim was observed for these specimens. In this case, hydrides were precipitated uniformly during the cooling stage of the hydrogenation test.

The deposition of a chromium coating on the outer surface of RUW specimens can be used as a barrier layer for hydrogen permeation. The same result was found in several studies [25,32]. We found that Cr-coated RUW specimens have lower hydrogen absorption rates and higher activation energy compared to uncoated ones (Table 1). Indeed, the lower hydrogen concentration was found in coated specimens after tests at 360 and 450 °C. As the Cr coating decreased hydrogen absorption, no hydride rim was found in the cross-section of welded specimens. These findings indicate the good barrier properties of the magnetron-deposited Cr coating to hydrogen permeation at temperatures simulating normal operation conditions. Moreover, the Cr-coated Zr alloy fuel rod suggested the deposition of a Cr coating on the surface of tube claddings should only occur when the ends of the rod remain uncoated [39]. The obtained results can be used as the rough estimations of a possible decrease in hydrogen absorption by Zr alloy rods under normal operation conditions, if it was fully coated by chromium. However, the Cr coating cannot significantly decrease the absorption rate of hydrogen at 900 °C (Figure 2c). It is more important that a higher hydrogen concentration was obtained in the Cr-coated specimen (3900 ppm) compared to the uncoated RUW (2700 ppm) as the Cr coating decreased the hydrogen output from the welded alloy during the cooling stage of the hydrogenation test. Such a trend can have a negative effect on the mechanical properties and integrity of welded Zr alloys after hydrogen exposure as the higher H concentration remains in the Cr-coated alloy.

The comparison of the hydrogenation behavior of RUW specimens and laser beam welds obtained in the previous study [25] showed that welding can cause a formation of transversely oriented hydrides in welded zones of specimens during hydrogenation procedures. In both types of welding, RUW and LBW, Cr coating deposition via magnetron sputtering can decrease such types of hydride precipitations in the case of low-temperature hydriding (360–450 °C). This can be considered as a one of the main advantages of the fully Cr-coated nuclear fuel rod compared to the uncoated one at temperatures of normal operation. Moreover, RUW specimens usually have some non-regularities (weld burr) on the surface in the weld zone due to an excess of liquid metal pressed in an outer surface during such types of welding. No presence of localized hydrides in cross-sections of Cr-coated specimens after hydrogenation at 360 and 450 °C indicated that the magnetron deposition of a 9.8 μm thick Cr coating can prevent the fast hydriding of welded Zr alloys in such regions. At the higher hydrogenation temperature (900 °C), the barrier properties of Cr coating decreases, and therefore, no considerable difference was found between the hydrogenation behavior of Cr-coated and uncoated RUW specimens.

5. Conclusions

Resistance upset welds of an E110 zirconium alloy without and with a 9.8 μm thick Cr coating deposited on its outer surface was studied in the temperature range of 360–900 °C in pure hydrogen atmosphere. The following conclusions were obtained:

1. Due to high hydrogen absorption rates of uncoated RUW specimens, a hydride rim can be formed in its outer surface at 360 and 450 °C. Chromium coating can decrease

the absorption rate by one order of magnitude and eliminate the growth of the hydride rim during the considered time of hydrogenation tests.
2. The influence of Cr coating on the hydrogen absorption rate in RUW specimens is noticeably decreased during hydrogenation at 900 °C. The Cr-coated RUW specimen has a higher residual concentration of hydrogen (3900 ppm) since hydrogen output from the welded alloy is slowed down by the coating during the cooling stage.
3. Welding can cause a formation of radially oriented hydrides in the welded zone of RUW specimens during hydrogenation. The coating deposition of Cr limits the formation of hydrides with such an orientation under low-temperature hydriding (360–450 °C).

Author Contributions: E.K.: Conceptualization, Investigation, Formal Analysis, Methodology, Writing—Review and Editing; K.G.: Visualization, Writing—Original Draft; V.K.: Investigation, Funding Acquisition; N.K.: Investigation; D.S.: Conceptualization, Investigation, Data Curation, Formal Analysis, Methodology, Writing—Review and Editing. All authors have read and agreed to the published version of the manuscript.

Funding: The reported study was supported by the Russian Science Foundation, grant number 19-79-10116.

Institutional Review Board Statement: Not applicable.

Informed Consent Statement: Not applicable.

Data Availability Statement: The data presented in this study are available on request from the corresponding author.

Acknowledgments: The authors thank Maxim Krinitcyn for the optical microscopy analysis.

Conflicts of Interest: The authors declare no conflict of interest.

References

1. Charit, I.; Murty, K.L. Creep behavior of niobium-modified zirconium alloys. *J. Nucl. Mater.* **2008**, *374*, 354–363. [CrossRef]
2. Allen, T.R.; Konings, R.J.M.; Motta, A.T. Corrosion of zirconium alloys. *Com. Nucl. Mater.* **2012**, *5*, 49–68.
3. Zinkle, S.J.; Terrani, K.A.; Gehin, J.C.; Ott, L.J.; Snead, L.L. Accident tolerant fuels for LWRs: A perspective. *J. Nucl. Mater.* **2014**, *448*, 374–379. [CrossRef]
4. Kane, K.; Bell, S.; Capps, N.; Garrison, B.; Shapovalov, K.; Jacobsen, G.; Deck, C.; Graening, T.; Koyanagi, T.; Massey, C. The response of accident tolerant fuel cladding to LOCA burst testing: A comparative study of leading concepts. *J. Nucl. Mater.* **2023**, *574*, 154152. [CrossRef]
5. Tang, C.; Stueber, M.; Seifert, H.J.; Steinbrueck, M. Protective coatings on zirconium-based alloys as accident-tolerant fuel (ATF) claddings. *J. Corros. Rev.* **2017**, *35*, 3.
6. Wang, W.; Zhang, G.; Wang, C.; Wang, T.; Li, T. Construction of chromium coatings with (200) preferred orientation and exploration the high-temperature steam oxidation properties. *J. Nucl. Mater.* **2022**, *563*, 153660. [CrossRef]
7. Yueh, K.; Terrani, K.A. Silicon carbide composite for light water reactor fuel assembly applications. *J. Nucl. Mater.* **2014**, *448*, 380–388. [CrossRef]
8. Brachet, J.C.; Urvoy, S.; Rouesne, E.; Nony, G.; Dumerval, M.; Saux, M.L.; Ott, F.; Michau, A.; Schuster, F.; Maury, F. DLI-MOCVD Cr_xC_y coating to prevent Zr-based cladding from inner oxidation and secondary hydriding upon LOCA conditions. *J. Nucl. Mater.* **2021**, *550*, 152953.
9. Dryepondt, S.; Unocic, K.A.; Hoelzer, D.T.; Massey, C.P.; Pint, B.A. Development of low-Cr ODS FeCrAl alloys for accident-tolerant fuel cladding. *J. Nucl. Mater.* **2018**, *501*, 59–71. [CrossRef]
10. Zhao, S.; Liu, C.; Li, Z.; Zhang, W.; Xiang, Y.; He, H.; He, L.; Yang, H.; Liu, N.; Chang, H.; et al. Effect of N content on microstructure and properties of (AlTiCrNiTa)N coatings for accident-tolerant fuels. *J. Intermet.* **2022**, *151*, 107728. [CrossRef]
11. Zeng, S.; Li, P.; Tian, J.; Chen, C.; Meng, Y.; Zhu, C.; Shen, H.; Han, X.; Zhang, H. Influence of Al content on the oxidation behavior of CrAl coating on Zry-4 alloys in 1200 °C steam. *Corros. Sci.* **2022**, *198*, 110115. [CrossRef]
12. Li, Z.; Li, Y.; Liu, S.; Wu, L.; Qin, W.; Wu, X. Enhancement of oxidation resistance of Cr/CrN composite coating on Zr-4 surface by high lattice-matched interfacial Engineering. *J. Nucl. Mater.* **2023**, *574*, 154162. [CrossRef]
13. Wang, X.; Liao, Y.; Xu, C.; Guan, H.; Zhu, M.; Gao, C.; Jin, X.; Pang, P.; Liao, B.; Xue, W. Steam oxidation behavior of ZrO_2/Cr-coated pure zirconium prepared by plasma electrolytic oxidation followed by filtered cathodic vacuum arc deposition. *J. Alloys Compd.* **2021**, *883*, 160798. [CrossRef]
14. Syrtanov, M.S.; Kashkarov, E.B.; Abdulmenova, A.V.; Sidelev, D.V. High-temperature oxidation of Zr-1Nb zirconium alloy with protective Cr/Mo coating. *Surf. Coat. Technol.* **2022**, *439*, 128459. [CrossRef]

15. Brachet, J.C.; Idarraga-Trujillo, I.; Le Flem, M.; Le Saux, M.; Vandenberghe, V.; Urvoy, S.; Rouesne, E.; Guilbert, T.; Toffolon-Masclet, C.; Tupin, M.; et al. Early studies on Cr-Coated Zircaloy-4 as enhanced accident tolerant nuclear fuel claddings for light water reactors. *J. Nucl. Mater.* **2019**, *517*, 268–285.
16. Hyun-Gil, K.; Il-Hyun, K.; Yang-Il, J.; Dong-Jun, P.; Jeong-Yong, P.; Yang-Hyun, K. Adhesion property and high-temperature oxidation behavior of Cr-coated Zircaloy-4 cladding tube prepared by 3D laser coating. *J. Nucl. Mater.* **2015**, *465*, 531–539.
17. Motta, A.; Long-Qing, C. Hydride formation in zirconium alloys. *JOM* **2012**, *64*, 1403–1408. [CrossRef]
18. Desquines, J.; Drouan, D.; Guilbert, S.; Lacote, P. Embrittlement of pre-hydrided Zircaloy-4 by steam oxidation under simulated LOCA transients. *J. Nucl. Mater.* **2016**, *469*, 20–31. [CrossRef]
19. Pshenichnikov, A.; Stuckert, J.; Walter, M. Microstructure and mechanical properties of Zircaloy-4 cladding hydrogenated at temperatures typical for loss-of-coolant accident (LOCA) conditions. *Nucl. Eng. Des.* **2015**, *283*, 33–39. [CrossRef]
20. Le Hong, T.; Turque, I.; Brachet, J.C.; Crepin, J.; Andre, G.; Barres, Q.; Guillou, R.; Toffolon-Masclet, C.; Joubert, J.M.; Le Saux, M. Phase transformations during cooling from the β_{Zr} phase temperature domain in several hydrogen-enriched zirconium alloys studied by in situ and ex situ neutron diffraction. *Acta Mater.* **2020**, *199*, 453–468.
21. Daub, K.; Nieuwenhove, R.V.; Nordin, H. Investigation of the impact of coatings on corrosion and hydrogen uptake of Zircaloy-4. *J. Nucl. Mater.* **2015**, *467*, 260–270. [CrossRef]
22. Kashkarov, E.B.; Nikitenkov, N.N.; Sutygina, A.N.; Obrosov, A.; Manakhov, A.; Polčák, J.; Weiß, S. Hydrogen absorption by Ti-implanted Zr-1Nb alloy. *Int. J. Hydrogen Energy* **2018**, *43*, 2484–2491.
23. Usui, T.; Sawada, A.; Amaya, M.; Suzuki, A.; Chikada, T.; Terai, T. SiC coating as hydrogen permeation reduction and oxidation resistance for nuclear fuel cladding. *J. Nucl. Sci. Technol.* **2015**, *52*, 1318–1322. [CrossRef]
24. Tang, C.; Grosse, M.K.; Trtik, P.; Steinbrück, M.; Stüber, M.; Seifert, H.J. H_2 permeation behavior of Cr_2AlC and Ti_2AlC max phase coated Zircaloy-4 by neutron radiography. *Acta Polytech.* **2018**, *58*, 69–76. [CrossRef]
25. Kashkarov, E.B.; Kudiiarov, V.N.; Kurdyumov, N.; Krinitcyn, M.G.; Sidelev, D.V. Hydrogenation behavior of Cr-coated laser beam welds of E110 zirconium alloy. *J. Nucl. Mater.* **2022**, *570*, 153980.
26. Sidelev, D.; Ruchkin, S.; Kashkarov, E. High-Temperature Oxidation of Cr-Coated Resistance Upset Welds Made from E110 Alloy. *Coatings* **2021**, *11*, 577. [CrossRef]
27. Sidelev, D.V.; Poltronieri, C.; Bestetti, M.; Krinitcyn, M.G.; Grudinin, V.A.; Kashkarov, E.B. A comparative study on high-temperature air oxidation of Cr-coated E110 zirconium alloy deposited by magnetron sputtering and electroplating. *Surf. Coat. Technol.* **2022**, *433*, 128134. [CrossRef]
28. Kashkarov, E.B.; Nikitenkov, N.N.; Sutygina, A.N.; Syrtanov, M.S.; Vilkhivskaya, O.V.; Pryamushko, T.S.; Kudiiarov, V.N.; Volesky, L. Effect of titanium ion implantation and deposition on hydrogenation behavior of Zr-1Nb alloy. *Surf. Coat. Technol.* **2016**, *308*, 2–9. [CrossRef]
29. Terrani, K.A.; Balooch, M.; Wongsawaeng, D.; Jaiyen, S.; Olander, D.R. The kinetics of hydrogen desorption from and adsorption on zirconium hydride. *J. Nucl. Mater.* **2010**, *397*, 61–68. [CrossRef]
30. Steinbrück, M. Hydrogen absorption by zirconium alloys at high temperatures. *J. Nucl. Mater.* **2010**, *397*, 61–68. [CrossRef]
31. Kurskii, R.A.; Safonov, D.V.; Rozhkov, A.V.; Zabusov, O.O.; Frolov, A.S.; Kuleshova, E.A.; Alekseeva, E.V.; Bragin, A.S.; Vasil'eva, E.A.; Gaiduchenko, A.B.; et al. Reorientation of Hydrides in Unirradiated Clad Tubes Made of Alloy E110 under Conditions Simulating Long-Term Dry Storage of Spent Nuclear Fuel. *Phys. Met. Metallogr.* **2021**, *122*, 861–868. [CrossRef]
32. Kim, J.-S.; Kim, H.-A.; Kang, S.-Y.; Kim, Y.-S. Effects of hydride rim on the ductility of Zircaloy-4 cladding. *J. Nucl. Mater.* **2019**, *523*, 283–390. [CrossRef]
33. Kashkarov, E.B.; Gusev, K.S.; Ashikhmin, D.A.; Abdulmenova, A.V.; Sidelev, D.V. Oxidation and Mechanical Behavior of Cr-Coated Laser Beam Welds Made from E110 Zirconium Alloy. *Coatings* **2022**, *12*, 1623. [CrossRef]
34. Yang, Z.B.; Liao, J.J.; Qiu, S.Y.; Cheng, Z.Q.; Liu, H.; Wu, Z.P.; Qiu, J.; Gao, B. Effect of Final Annealing Temperature on Corrosion Resistance of SZA-6 Zirconium Alloy Cladding Tubes. *Mater. Sci. Forum* **2019**, *944*, 488–498. [CrossRef]
35. Semenov, A.N.; Plyshevskii, M.I.; Melyukov, V.V. Properties of welded joints from alloy Zr-2.5%Nb after electron-beam local thermocycling. *Met. Sci. Heat Treat.* **2014**, *55*, 670–674. [CrossRef]
36. Carpenter, G.J.C. The dilatational misfit of zirconium hydrides precipitated in zirconium. *J. Nucl. Mater.* **1973**, *48*, 264–266. [CrossRef]
37. Wang, S.; Li, S.; Li, R.; Wang, Y.; Xu, N.; Xue, F.; Bai, G.; Wang, Y.-D. Microscopic stress and crystallographic orientation of hydrides precipitated in Zr-1Nb-0.01Cu cladding tube investigated by high-energy X-ray diffraction and EBSD. *J. Nucl. Mater.* **2020**, *542*, 152534. [CrossRef]
38. Chernyayeva, T.P.; Ostapov, A.V. Hydrogen in zirconium part 1. *Probl. At. Sci. Technol.* **2013**, *87*, 16–32.
39. Bischoff, J.; Delafoy, C.; Vauglin, C.; Barberis, P.; Roubeyrie, C.; Perche, D.; Duthoo, D.; Schuster, F.; Brachet, J.-C.; Schweitzer, E.W.; et al. AREVA NP's enhanced accident-tolerant fuel developments: Focus on Cr-coated M5 cladding. *Nucl. Eng. Technol.* **2018**, *50*, 223–228. [CrossRef]